J. Condensed Matter Nucl. Sci. 6 (2012) 217–240

Research Article

Spectral and Temporal Characteristics of X-ray Emission from Metal Electrodes in a High-current Glow Discharge

A.B. Karabut*

Samar+ COMPANY, Belay Dacha, 13, ap. 54, city Kotelniky, Moscow Region, 140055, Russia

E.A. Karabut

Moscow Power Engineering Institute (Technical University)

P.L. Hagelstein

Massachusetts Institute of Technology, USA

Abstract

We have observed X-ray emission from metal cathodes in high-current (up to 500 mA) glow discharge experiments in the spectral range from 600 eV to 6 keV. The effect has been seen with a variety of different metal cathodes (including Al, Sc, Ti, V, Ni, Nb, Zr, Mo, Pd, Ta, W, and Pt), as well as with different gasses (including D_2, H_2, Kr, Ar, and Xe) at low pressure (10 torr). We have observed both diffuse and collimated X-ray emission. Diffuse emission occurs in bursts of X-rays; with up to 10^5 bursts per second, with up to 10^6 photons per burst. Collimated X-ray emission appears in the form of beamlets directed normal to the cathodes surface with a very small angular divergence; with up to 10^4 bursts per second, and up to 10^{13} photons overall. Switching off the glow discharge current produces substantial X-ray bursts in these experiments; and we see some bursts during the discharge, and up to 20 h after switch off. We present results from a variety of diagnostics, including: pinhole camera imaging; thermo-luminescent detector measurements; time-resolved scintillator measurements; and a curved mica spectrometer to register X-ray spectra. The spectra of the collimated X-rays shows a strong broad emission feature that is centered near 1.5 keV in many experiments. Line emission is sometimes observed in addition along with the broad feature.

Keywords: Collimated X-ray, Diffuse X-ray emission, Excited phonon mode, Glow discharge device, X-ray spectra

1. Introduction

Our group has studied low energy nuclear reactions (LENR) in glow discharge experiments for many years. Glow discharges are relevant to such studies as deuterium (or hydrogen) can be loaded into Pd (or into other metals) by the

*E-mail: karab.ab@mail.ru; Tel.: (495) 5508129; Fax: (495) 5508129

discharge under low pressure and high current conditions. We have seen a variety of anomalies in our glow discharge experiments, including excess heat, charged particle emission, gamma emission, helium production, tritium, changes in the cathode composition, as well as residual radiation [1]. Some years ago we noticed a new effect in which collimated X-ray emission was observed in a beam normal to the cathode surface [2,3], and we have focused considerable effort on the effect subsequently [4–7]. This effect is interesting for a variety of reasons. In some experiments the X-ray emission is observed at higher energies (up to 10 keV) than would be expected given the discharge voltage (1–2 kV). The emission can be seen after the discharge has been turned off, under conditions where there is no discharge current. That the X-ray emission is collimated is significant, and we might expect that the effect itself can tell us something about the physical processes involved in LENR reactions.

In this work we review earlier collimated X-ray experimental results, including pinhole camera measurements, thermal luminescence detector measurements, and time-resolved scintillator/PMT measurements. Then we present our new results on the emission spectra, taken with a curved mica crystal spectrometer.

2. Glow Discharge Experiment

The measurements were carried out using a glow discharge device consisting of a water-cooled vacuum chamber, and cathode and anode assemblies as shown in Fig. 1(a). Cathode heating is an issue under high-current conditions, so we designed the cathode assembly so that cathode samples could be attached to a water-cooled surface. We studied cathode samples made out of a variety of different metals, including Al, Sc, Ti, Ni, Nb, Zr, Mo, Pd, Ta, W, Pb and Pt. Discharge experiments were run using different gasses as well, including D_2, H_2, He, Kr and Xe.

The power supply is designed to provide the glow discharge with periodic-pulse direct current, and permits the generation of desired current forms (of various pulse length and pulse period) to obtain the required current voltage operating conditions. The power supply consists of an autotransformer; a step-up transformer; a rectifier; a storage capacitor; a ballast resistor; and a high voltage transistor switch. The power supply produces direct pulse-periodic current of rectangular shape of pulse, illustrated in Fig. 1(b). In the experiments, we used pulse durations from 0.1 to 1.0 ms; and a period from 0.3 up to 100 ms. The glow discharge conditions were: current (amplitude), from 30 up to 300 mA; voltage, from 1500 to 4300 V; and gas pressure in the discharge chamber, from 3 to 5 Torr. As mentioned above, X-ray measurements were carried using an X-ray pinhole camera, thermo-luminescent detectors, and scintillation detectors with photomultiplier. The energy spectrum of the X-ray emission was obtained using a curved mica crystal spectrometer. The cathode samples made of Pd and other metals were placed on a cathode-holder above which a window for output penetrating radiation was provided. Various detectors were installed above the window to measure the output penetrating radiation.

3. Pinhole Camera and Results

Since the X-ray emission from the cathode was so intense, it was possible to use it to obtain an X-ray pinhole camera image of the cathode. The experimental set up is shown schematically in Fig. 2a. In order to check whether the emission is due to X-rays, a transverse 0.3 T magnetic field was used to deflect charged particles. The image of Fig. 2b shows the cathode (9 mm in diameter) and was taken with no magnetic field; the image of Fig. 2(c) was taken with a magnetic field. If the image were due to charged particles, such as electrons, then the image would have disappeared. One can see that the magnetic field does not change the cathode image qualitatively, so we conclude that the image is due to X-ray radiation.

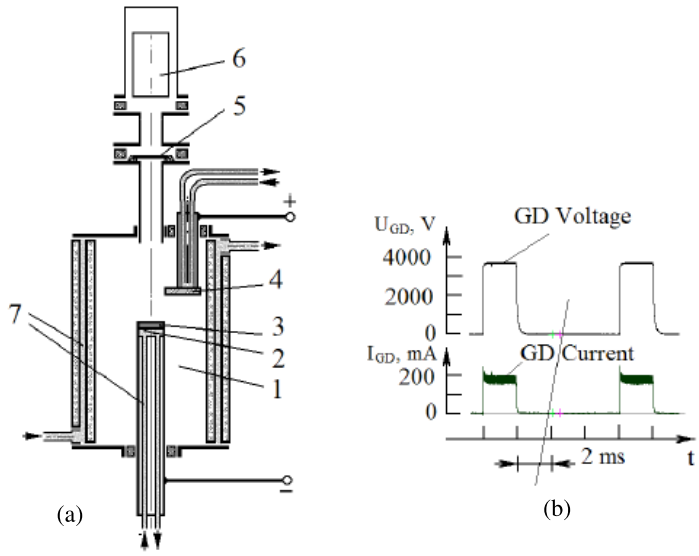

Figure 1. Schematic representation of the experiment. (a). Glow discharge device, 1 – discharge chamber, 2 – cathode holder, 3 – cathode sample, 4 – anode, 5 – Be foil screens, 6 – X-ray detectors different kind (pinhole, TLD detectors, scintillator- photomultiplier, spectrometer), objective, 7 –cooling water; (b) glow discharge voltage and current pulses.

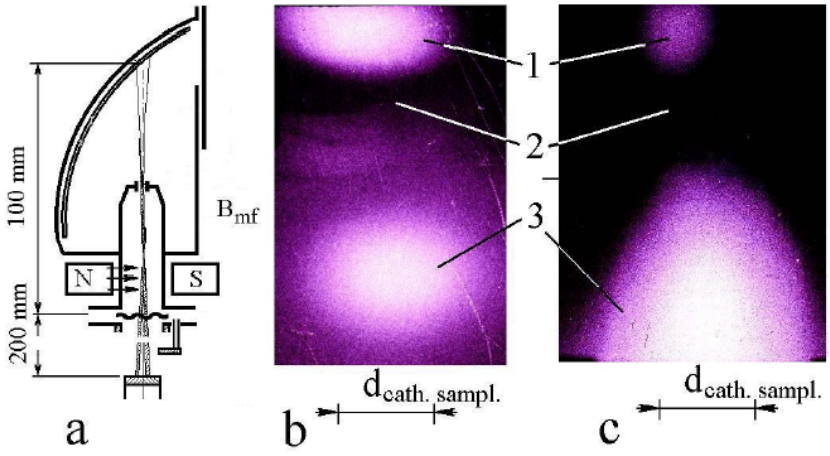

Figure 2. (a) Schematic of the X-ray pinhole camera experiment. The objective with 2.0 mm diameter closes by the 15 μm Be shield. Data is shown for a Pd cathode and D_2 gas, with a discharge current of 150 mA, a voltage of 1850 V, and with an exposure time of 10 000 s; (b) X-ray image without a cross magnetic field; (c) X-ray image with a cross magnetic field of 0.3 T. The image is positive, showing the anode (1), discharge plasma area (2) and cathode (3).

4. TLD Detector and Results

We used thermo-luminescent detectors (TLD) (based on crystalline Al_2O_3) to study the energy and intensity of the X-ray emission. Thermo-luminescence in Al_2O_3 is well known and has been studied in recent years in [8,9]. We used Al_2O_3 disk detectors that were 5 mm in diameter and 1 mm thick. Exposure with the 661.5 keV gamma line from a ^{137}Cs calibration source was used for calibration, assuming that the response to the total radiation energy would be similar for gamma radiation as for X-ray radiation. A Harshaw model 2080TL-PICOPROCESSOR was used for analysis of the exposed crystals. We built a seven channel TLD detector, with Be foils of different thicknesses (15, 30, 60, 105, 165, 225, 225, 300 μm) in front of different TLD detectors. Additionally, two TLD detectors were arranged outside the camera for the registration of background value of the emission dose. The main component of the X-ray emission energy is in the range of 1.3–1.8 keV, but there is a component with a higher energy too (Fig. 3(b)). TLD measurements show that X-ray radiant intensity from the cathode surface increases exponentially with the increase in the glow discharge voltage (Fig. 3(c)).

5. Scintillation Detector and Results

We made use of scintillation detectors with photomultipliers to study the time-dependence of the X-ray emission, and also the X-ray energy and spatial dependence. We used organic scintillators based on polymethylmetacrylate (PMMA) with a de-excitation time of 3–5 ns. The optical signal from the PMMA was detected using a photomultiplier (PM); the signal from the PM was transferred to a fast preamplifier, and then to a two-channel computer digital oscilloscope with the frequency limit of 50 MHz per channel.

We used three variants of the discharge chamber (with different extensions of the vacuum chamber) for X-ray

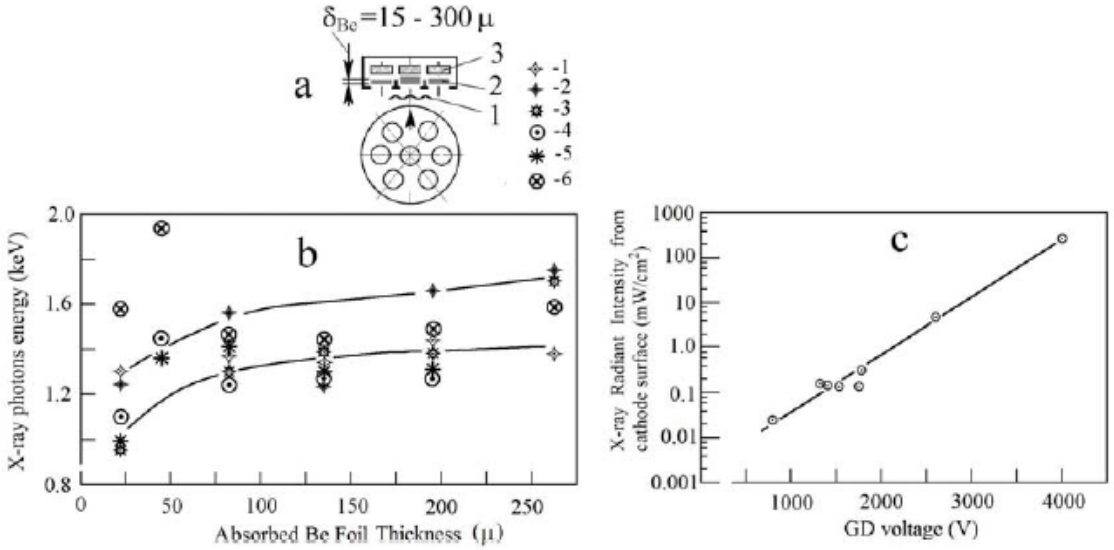

Figure 3. (a) The seven-channel TLD spectrometer; (b) the X-ray dose absorbed by TLD detectors covered with Be foil with the different thickness (where the discharge voltage for the different experiments is: 1 – 1750 V, 2 – 1770 V, 3 – 1650 V, 4 – 1530 V, 5 – 1400 V, 6 – 1250 V); (c) dependence of the X-ray emission energy on the discharge voltage from TLD measurements. These experiments were done with a Pd cathode, D_2 gas, with a current of 200 mA, and an exposure time of 6000 s.

detection (as described in [3]). In the first variant, the PMMA/PM detector was placed 21 cm from the cathode surface, and the diameter of the extension (for extracting the radiation) was 1.7 cm. In the second variant, the PMMA/PM detector was placed 70 cm from the cathode, and the extension diameter was 3.2 cm. For determining whether the radiation is charged particle or electromagnetic radiation, the third variant included a 0.3 T magnetic field 35 cm from the cathode oriented perpendicular to the beam. From the experiments with the magnetic field it was found that the collimated radiation is not charged particles.

We detected both diffuse and collimated X-rays in these experiments. Diffuse X-ray emission occurs mainly when the discharge is on (see Fig. 4(a)), and occurs in flashes some msec after switching off the current. The intensity of this diffuse radiation goes down as $1/r^2$ away from the cathode.

Collimated X-ray emission occurs during the discharge, and up to 100 ms after switching off the current. Under the certain parameters of discharge the generation of collimated X-rays occurs only some after turning off the discharge current (up to 20–30 beams after the each current pulse). The time-dependence of collimated X-ray emission correlated with the discharge switch off is illustrated in Fig. 4(b). Note that the bursts associated with the collimated X-rays are much more powerful than those associated with diffuse X-rays (the sensitivity of the PMMA/PM system was reduced by a factor of 2500 in the case of collimated X-rays). Collimated X-ray emission is also triggered by an increase in the value of discharge parameters, such as current, voltage, and the duration of the current pulse.

In Fig. 4(b) we denoted the delay time $\Delta\tau$ between the current switch off and the onset of a collimated X-ray burst. This delay time was studied in a series of experiments. Results for the delay time, and the associated number of bursts that occurred, are summarized in Fig. 5.

The average X-ray energy was determined in the PMMA/PM scintillator experiments by measuring the transmission through 15 and 30 μm Be foils, and matching the difference to the theoretical value. This was done by summing all pulses ($\Sigma A1_i$ and $\Sigma A2_i$) within a 1 s interval for the two cases (illustrated in Fig. 6). The average X-ray energy determined in this way for different cathode metals (between 1.2 and 2.0 keV) was found to be in good agreement with the average energy estimated from the TLD detector experiments, as indicated in Table 1. The number of photons was estimated as the energy of a burst divided by the average X-ray energy.

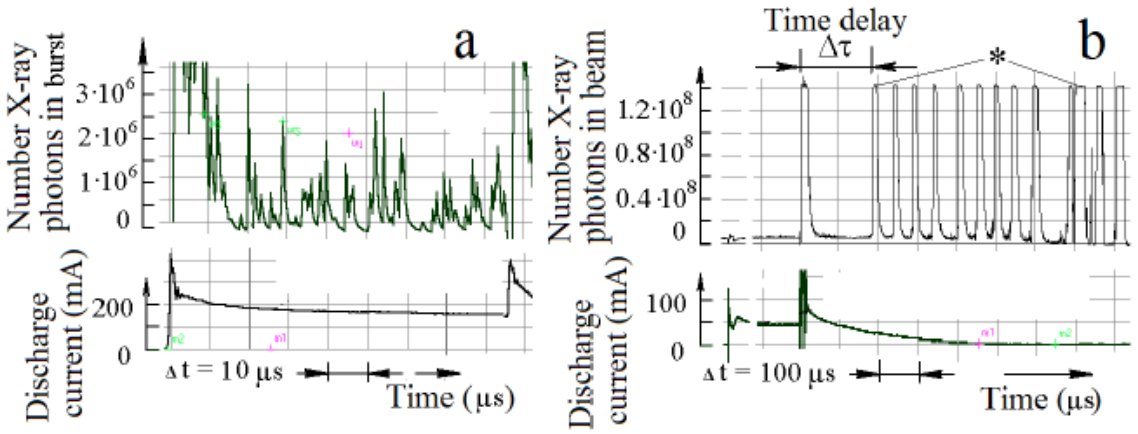

Figure 4. Typical oscillograms of the X-ray emission signal from the PMMA/PM scintillation detector. The cathode sample is Pd, run in a D_2 discharge; (a) diffuse radiation; (b) collimated radiation. The asterisk (*) signifies that the pulse peak was cut off by the amplifier discriminator.

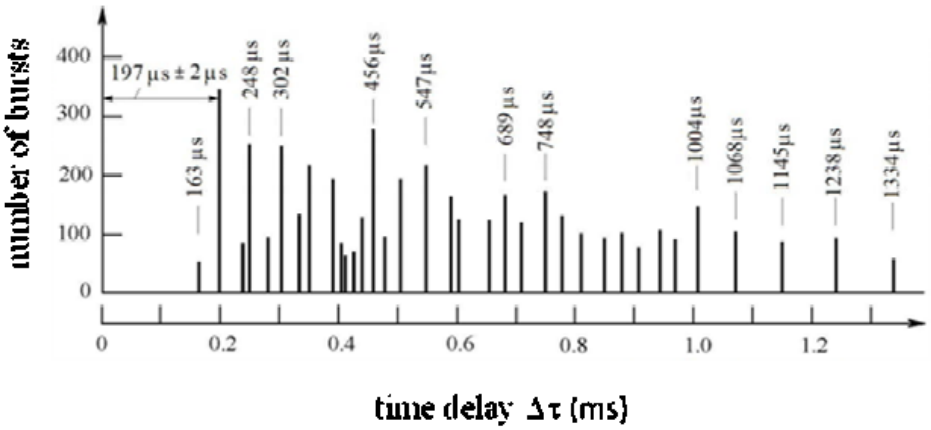

Figure 5. Results of a study of the number of bursts and their associated delay time from different experiments. The cathode for these experiments is Pd, the gas is D_2, and the current when the discharge is on is 50 mA.

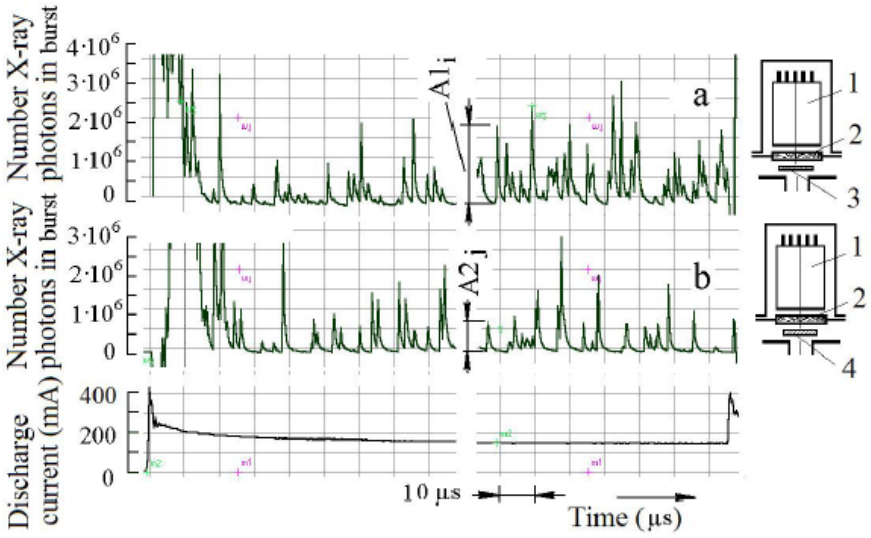

Figure 6. Typical oscillograms of X-ray emission from the PMMA/PM scintillator detector covered with Be foils with different thicknesses: (a) covered with a 15 μm Be foil; (b) covered with a 30 μm Be foil. In this case the cathode was Pd, the gas was D_2, and the discharge current was 150 mA.

Table 1. Average X-ray energy for different cathode materials.

Material of Cathode	Al	Sc	Ti	Ni	Mo	Pd	Ta	Re	Pt	Pb
Glow discharge voltage (V)	1650	1540	1730	1650	1420	1650	1600	1520	1650	1610
Glow discharge current (mA)	130	130	170	150	210	138	138	125	138	138
X-ray photons energy (keV)	1.54	1.26	1.45	1.91	1.48	1.98	1.62	1.36	1.47	1.36

6. X-ray Spectrometer and Spectral Features

X-ray emission spectra were measured using a bent mica crystal spectrometer as illustrated in Fig. 7; the mica crystal holder has a diameter of 50 mm, and the spectra are registered on X-ray film. Because of the spectrometer set up, the film records some of the beam directly, a specular reflected image, the first-order diffracted spectrum, and higher-order diffracted spectra with less efficiency. The direct X-ray beam signal appears in the highest energy part of the diffracted spectrum, causing an interference with the diffracted spectrum.

To determine the wavelength and energy from the diffraction angle θ, we used the (normal incidence) grating equation

$$m\lambda = d \sin\theta$$

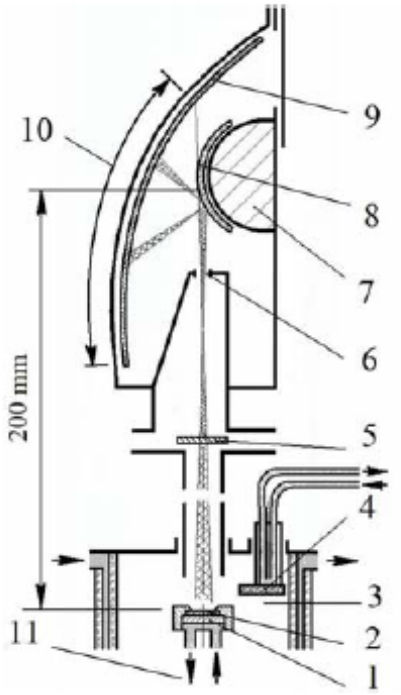

Figure 7. X-ray spectrometer; 1– cathode holder, 2– cathode sample, 3 – vacuum discharge chamber, 4 – anode, 5 –15 μ Be screen , 6 – input slit of spectrometer, 7 – crystals holder, 8 – curved mica crystal, 9 – X-ray film, 10 – area of reflection spectra , 11 – input and output cooling water.

where m is the spectrum order; λ stands for the X-ray wavelength; and d is the lattice constant of the mica crystal (d = 2.0 nm). (Note that the incident X-ray beam is not normal on the grating, so that this will introduce some error in the X-ray wavelengths and energies). The X-ray energy E is determined from

$$E(\text{keV}) = 1.235/\lambda(\text{nm}),$$

where E is in keV when the wavelength is expressed in nm.

The spectra were repeatedly recorded during the glow discharge operation with the exposure time 1–5 h, and some spectra were taken after the glow discharge current switch off (for up to 20 h). The X- ray negative films were scanned with 4800 dpi resolution points in color mode.

The spectra contains a variety of components, including a broad continuum, spectral lines, dark and light spots that are made up of multiple smaller spots, and finally separate dark and light spots. The collimated X-ray beams with small angular divergence were generally recorded as dark spots, but when the beam intensity was very high they appear white, (due to an effect known from the early days of photography as solarization). The continuum is diffuse, but originates from the cathode surface. Individual diffracted spectral lines are apparent in the spectra, and appear as conventional spectral lines since there is no source imaging in the spectrometer. Line emission from characteristic transitions in the heavy gas atoms (Ar, Kr and Xe) can be seen in some spectra. Line emission from characteristic transitions of the cathode metal atoms can be seen in some spectra.

The images of the spectra presented in what follows are negative.

6.1. Continuum spectra

We see a broad continuum signal between 0.6 and 6 keV (perhaps as high as 10 keV) which is diffuse (not collimated). The peak of this continuum appears between 1 and 2 keV, and is dependent on the cathode material. Examples are shown in Figs. 8–17. This emission is diffuse, and originates from the cathodes surface.

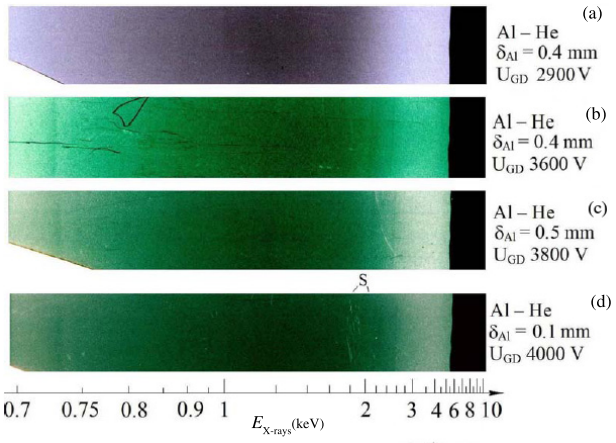

Figure 8. X-ray energy spectra from Al cathodes with different thickness (δ_{Al}) and different discharge voltages. The gas used in these experiments was He; U_{GD} is the glow discharge voltage; S denotes white solarization spots of photoemulsion from monenergetic X-ray beams with small angular divergence.

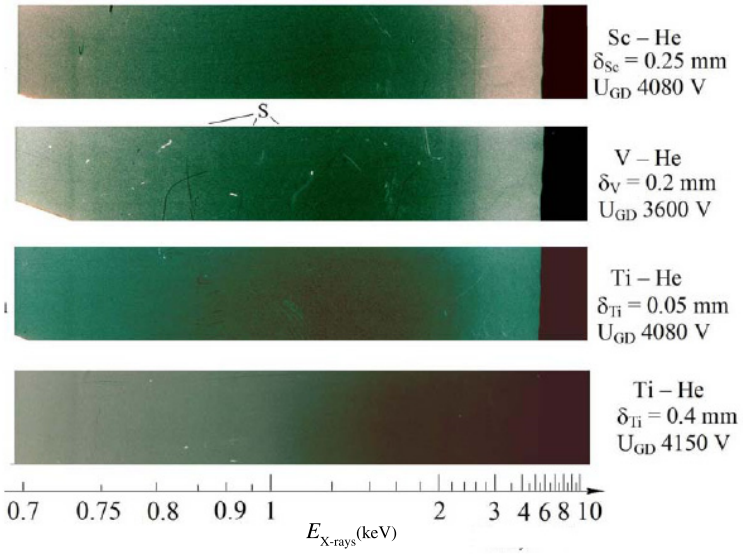

Figure 9. X-ray spectra from Sc, V and Ti cathodes with different thickness (δ) and different discharge voltages. The gas used in these experiments was He; U_{GD} is the glow discharge voltage; S denotes white solarization spots of photoemulsion from monenergetic X-ray beams with small angular divergence.

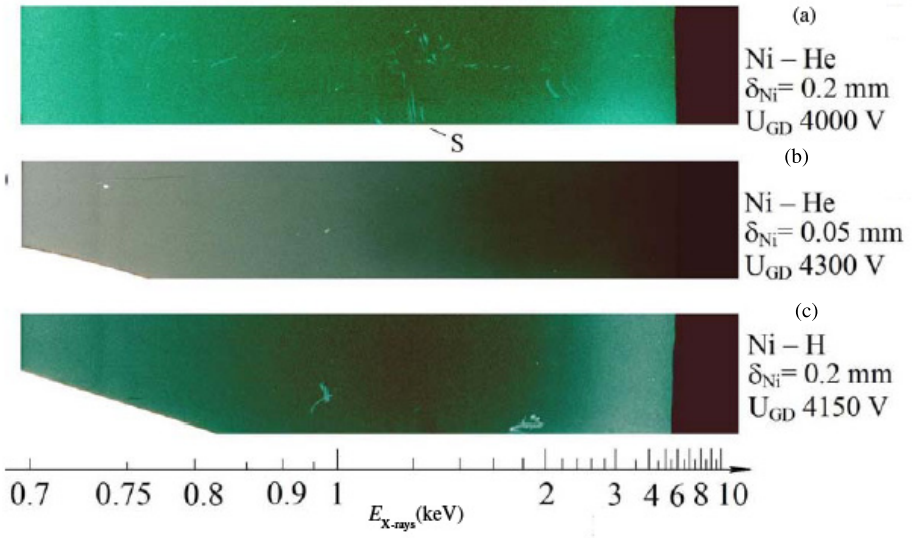

Figure 10. X-ray energy spectra from Ni cathodes with different thickness (δ_{Ni}) and different discharge voltages. The gas used in these experiments was He and H_2 as noted; U_{GD} is the glow discharge voltage; S denotes white solarization spots of photoemulsion from monenergetic X-ray beams with small angular divergence.

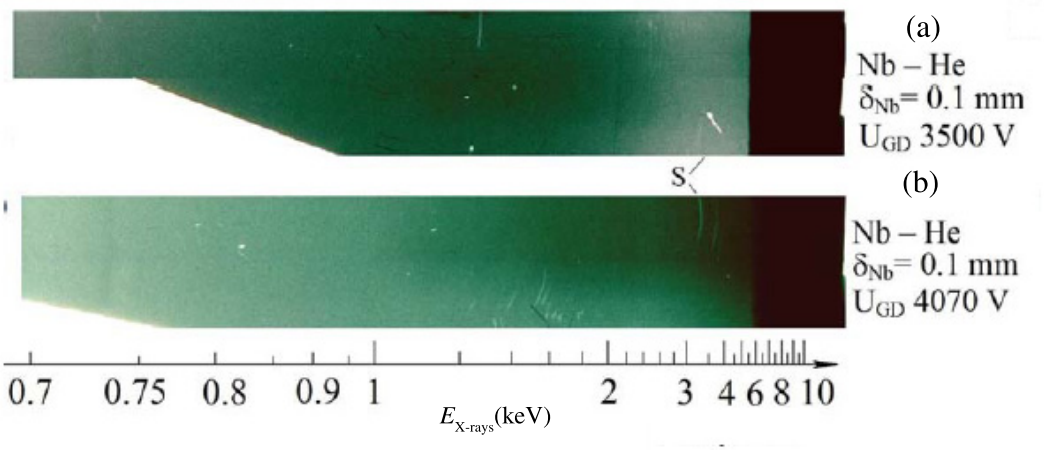

Figure 11. X-ray energy spectra from Nb cathodes at different discharge voltages. The gas used in these experiments was He; U_{GD} is the glow discharge voltage; S denotes white solarization spots of photoemulsion from monenergetic X-ray beams with small angular divergence.

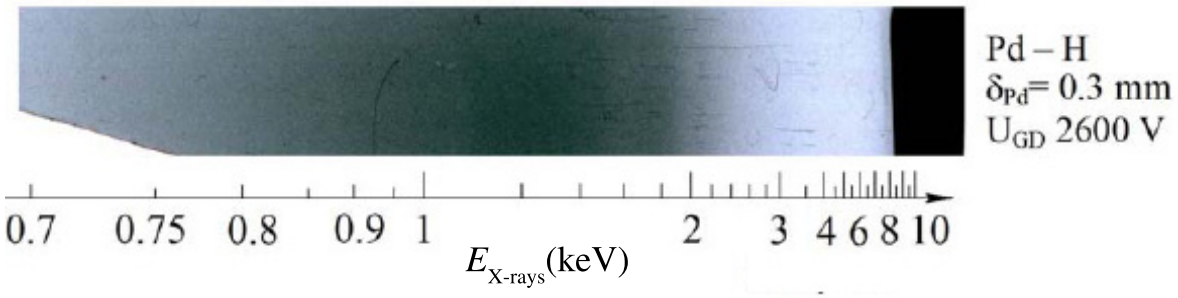

Figure 12. X-ray energy spectra from Pd cathode B H_2 discharge.

6.2. Spectra of collimated emission taken during discharge operation

Monoenergetic X-ray beams with small angular divergence were recorded as dark spots, and in case of very intense beams they turned white due to solarization of the photoemulsion. The term "solarization" comes from the early days of photography, and is an effect in which high intensity light produces a negative image (so that a dark spot become white) on the film. Examples of very bright X-ray beam emission taken during pulsed mode discharge operation are shown in Figs. 17–26.

A narrow beam with a fixed energy, direction, and origin will appear on the film after diffraction as a localized spot (see Fig. 20, and also Fig. 24, for examples). A change of direction during the emission, such as might be produced if the cathode surface moves, could result in a curve; if this slit were narrow, this would be expected to result in a vertical line (Fig. 23 shows a nearly vertical line, although the slit was not narrow); however, the slit used in these experiments was 6 mm wide, so that changes in the beam direction would alter the angle of incidence on the bent crystal causing what might look like a change in energy on the film.

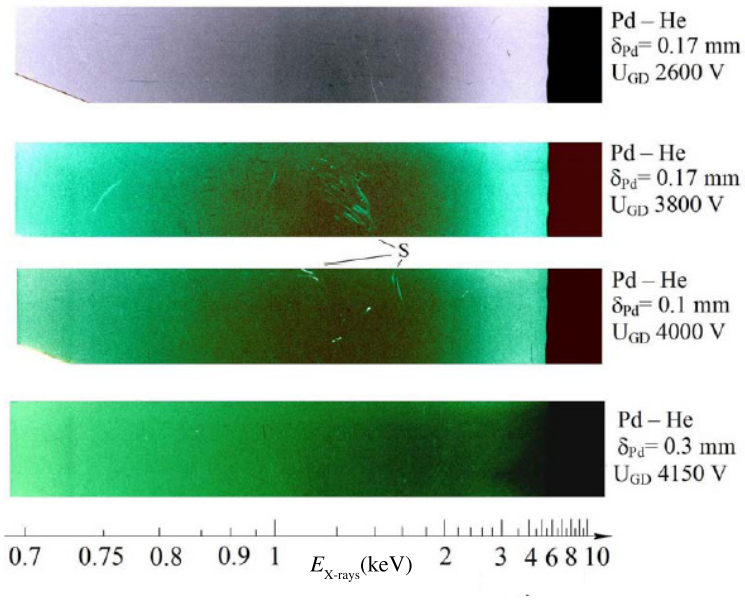

Figure 13. X-ray energy spectra from Pd cathodes with different thickness (δ_{Pd}) and different discharge voltages. The gas used in these experiments was He; U_{GD} is the glow discharge voltage; S denotes white solarization spots of photoemulsion from monenergetic X-ray beams with small angular divergence.

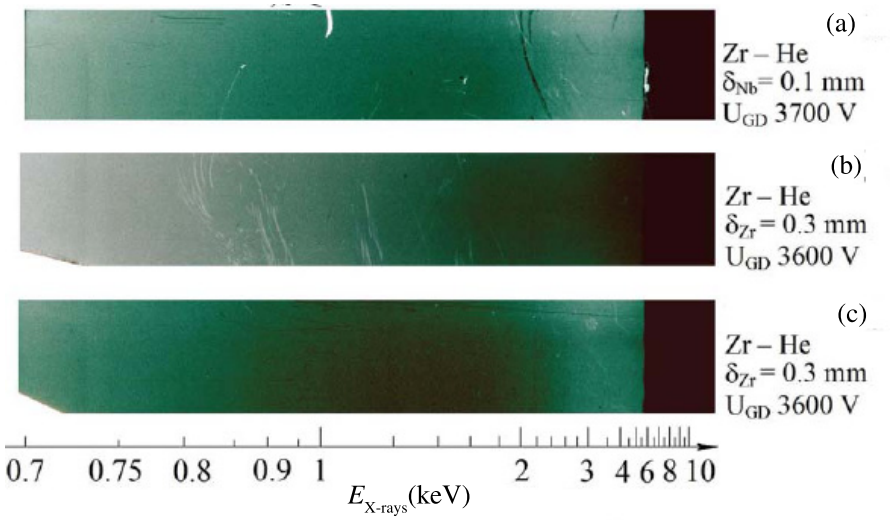

Figure 14. X-ray energy spectra from Zr cathodes with different thickness (δ_{Zr}) and different discharge voltages. The gas used in these experiments was He; U_{GD} is the glow discharge voltage; S denotes white solarization spots of photoemulsion from monenergetic X-ray beams with small angular divergence.

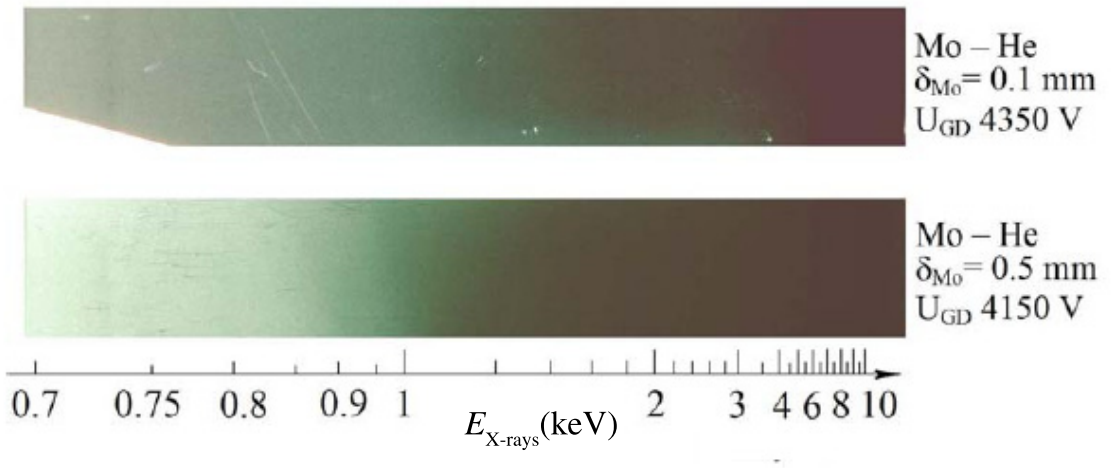

Figure 15. X-ray energy spectra from Mo cathodes with different thickness (δMo) and different discharge voltages. The gas used in these experiments was He; U_{GD} is the glow discharge voltage; solarization spots of photoemulsion from monenergetic X-ray beams with small angular divergence are apparent.

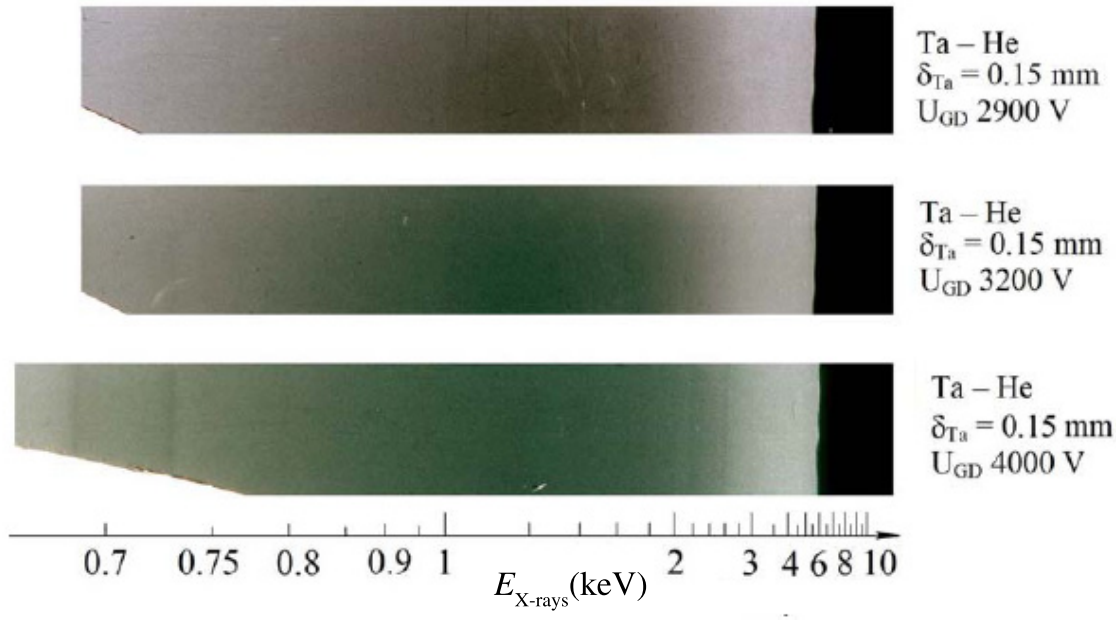

Figure 16. X-ray energy spectra from Ta cathodes at different voltages U_{GD}. He discharge.

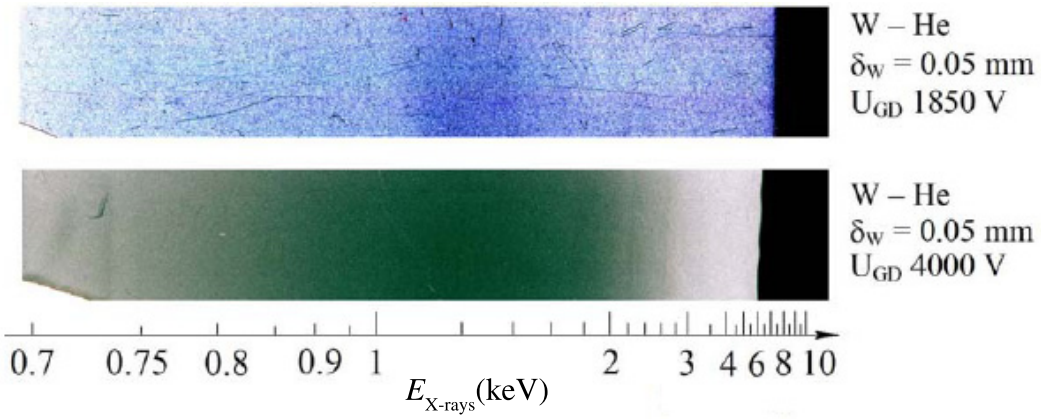

Figure 17. X-ray energy spectra from Mo cathodes at different voltages U_{GD} in He gas.

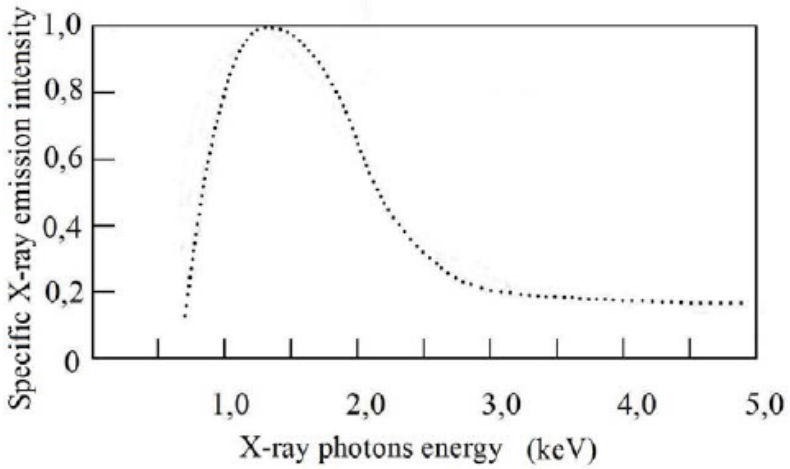

Figure 18. The X-ray continuum spectrum for a Pd cathode with D_2 gas, with a glow discharge voltage of 2600 V.

6.3. Spectra of collimated emission taken after discharge switch off

In the time resolved scintillator measurements, strong collimated emission occurs in bursts immediately following the switch off of the discharge. We noticed that emission can also occur an extended time after the discharge was turned off. In Figs. 27–32 we show examples of collimated monoenergetic X-ray beams that appeared after the discharge was switched off; data was collected for 20 h after switch off in the figures.

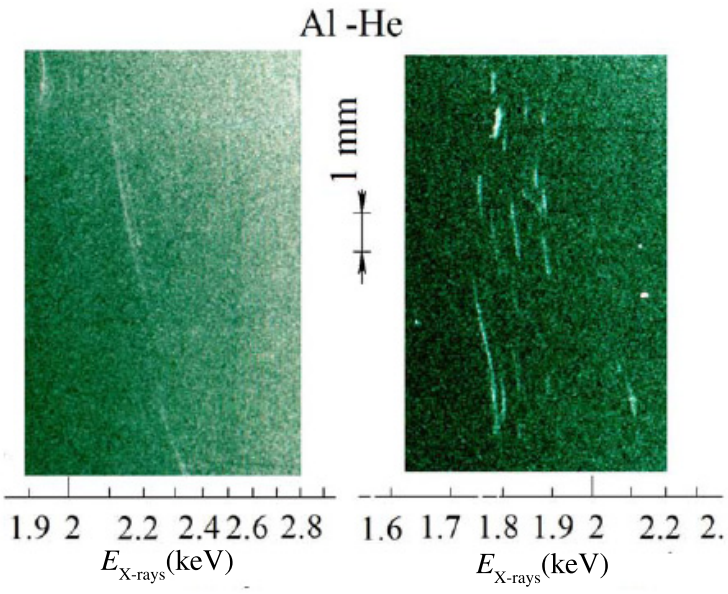

Figure 19. X-ray spectra showing collimated monoenergetic beams from Al cathodes with He gas.

6.4. X-ray spectra showing line emission taken during discharge operation

We observed characteristic X-ray K-shell line emission near 3 keV that could be associated with the gas in the case of Ar, as can be seen in Fig. 33. Electron beam excited Ar has been reported in the literature, and the K_α emission is dominant [10,11]. Similarly, when Kr gas is used we can see strong characteristic L-shell line emission in Fig. 34 (see [11] for the Kr line under electron beam excitation). In both cases this radiation appears to be sourced at or near the cathode surface, and not in the discharge. Characteristic L-shell emission from the cathode can be seen in the case of Zr and Mo cathodes (and perhaps the Pd cathode as well) in Fig. 35; theoretical and experimental spectra for electron beam bombardment of Mo is given in [12]. In all cases this diffuse radiation originates at (or near) the cathode surface.

7. Discussion and conclusion

Collimated X-ray emission in these glow discharge experiments constitutes a new and fundamental physical effect that has not been observed previously. Such an effect requires an explanation. In previous work we proposed that the collimated emission is due to X-ray lasing in the cathode. A problem with this proposal is that the creation of an X-ray laser requires a population inversion (or equivalent), which seems problematic since electronic lifetimes in the keV regime are very short, and since there seems to be no clear mechanism that could result in a population inversion.

There is an alternate approach, however, to the problem of developing a collimated beam in the X-ray regime. It is well known that a phased array of antennas (such as might be used for radar) can produce a collimated beam, and atoms and nuclei radiate individually as microscopic antennas. Hence, the experimental observation of collimated X-ray emission in these experiments suggests that there is some new mechanism which results in phase coherent excited states with keV energy (but no population inversion). This is a highly nontrivial accomplishment.

How might such phase coherent excitation be produced? Some colleagues have suggested that the electrons in the

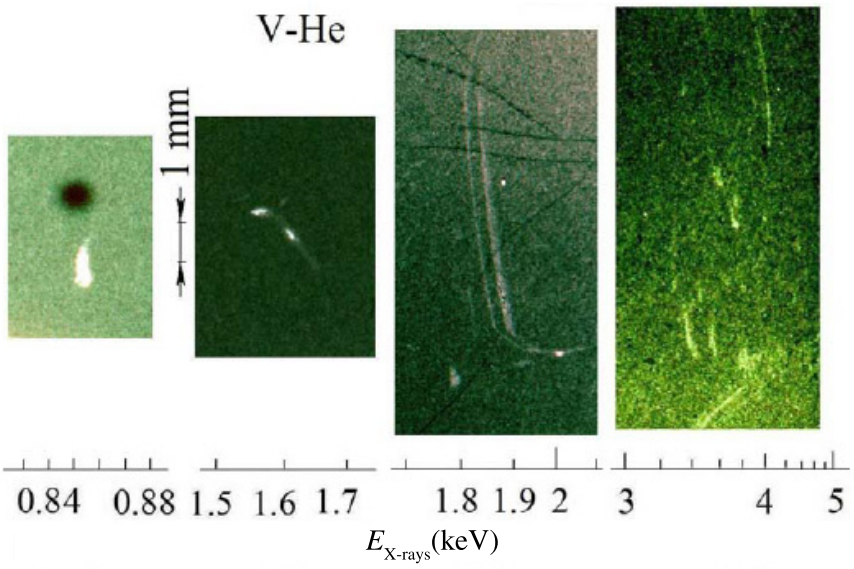

Figure 20. X-ray spectra showing collimated monoenergetic beams from V cathodes with He gas.

discharge will gain energy close to the applied voltage, which could cause excitation. While this is true in principle, collimated beams are seen after the discharge current is switched off (see Fig. 4), and also long after the discharge has been switched off (see Figs. 27–32). One would expect excitation caused by fast electrons to be strongest during the discharge. The collimated emission is sourced at the cathode surface, but energetic electrons impact the anode, and the corresponding radiation from the anode is blocked by the pinhole. Energetic ions impacting the anode could in principle cause electronic excitation (the energy is much too low for collisions producing nuclear excitation), but such an effect should be strongest during the discharge, not after.

There has been interest in the possibility that coherent energy exchange might be possible between a highly excited phonon mode, and an energetic nuclear transition [13,14]. If we consider such an approach as being relevant to collimated X-ray emission, then perhaps the first question might be whether there might exist a highly excited vibrational mode, preferably one that is uniform in the vicinity of the emitters. It can be noticed that a sharp current spike occurs when the current is switched off, which is likely to be associated with a local pressure spike on the cathode surface. The conjecture is that this can be effective in exciting the lowest compressional modes of the cathode.

It has been noted previously that ^{201}Hg has the lowest excitation energy from the ground state of all of the stable nuclei, with a transition energy of 1565 eV [15]. According to the models studied so far, it seems unlikely that coherent energy exchange can occur directly between this transition and the vibrational mode (since the coupling is far too weak). However, if there is another transition at higher energy that is strongly coupled, then we might expect energy exchange via a mechanism related to the model outlined in [16]. The stronger transition in this case would produce a mixing between the nuclear and phonon degrees of freedom, causing a spreading in the phonon distribution. Since the half life of the ^{201}Hg transition is short (about 81 ns according to [17]) we expect coherent energy exchange to occur while emission occurs, which would result in a broad line shape. This we might associate with the strong diffuse continuum feature seen in these experiments. Note that we would expect the least broadening to occur with the smallest phonon

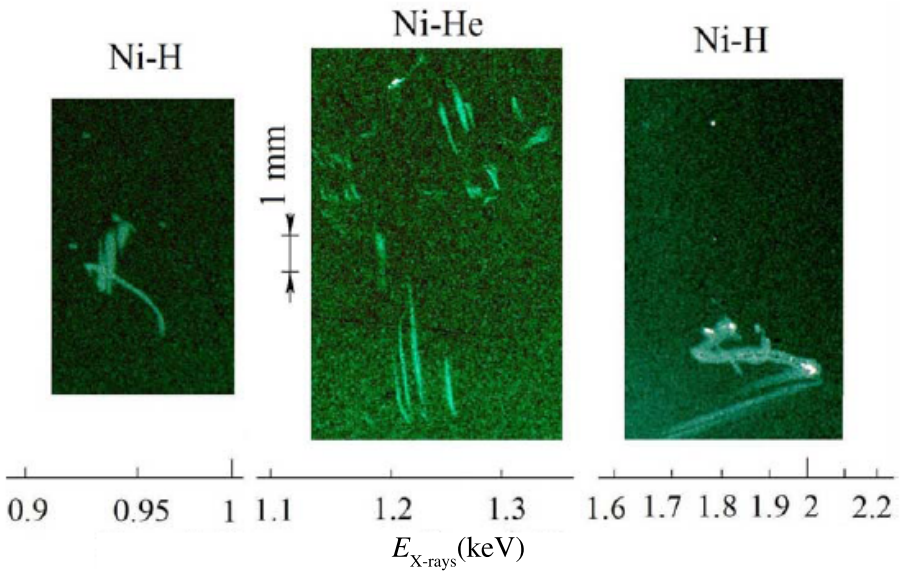

Figure 21. X-ray spectra showing collimated monoenergetic beams from Ni cathodes with H_2 and He gas.

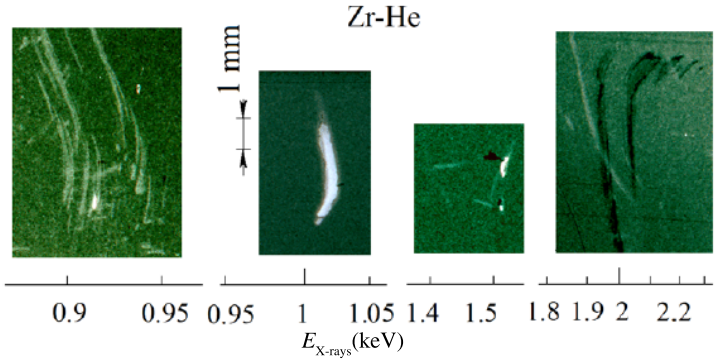

Figure 22. X-ray spectra showing collimated monoenergetic beams from Zr cathodes with He gas.

excitation; consequently our attention is drawn to the continuum in the lowest voltage example (1850 V) of Fig. 17, where the continuum seems narrower and more closely centered near about 1400 eV.

In this picture we would attribute the collimated X-ray beams to a phased array beam formation effect, in which ^{201}Hg nuclei are embedded randomly (but in phase) in the outer surface of the cathode. From preliminary simulation results, one observes that the phases can add up at sharp energy resonances (which can be different for different random samples) that fall within the broad emission line shape of the ^{201}Hg. If we include the effect of cathode photoabsorption

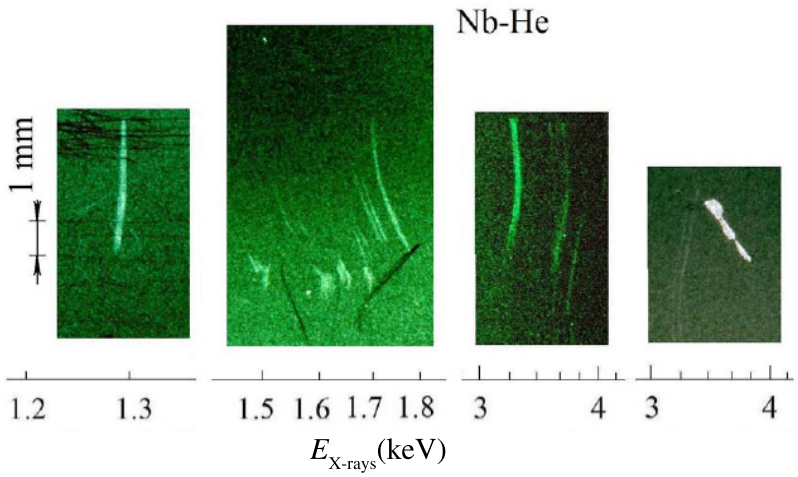

Figure 23. X-ray spectra showing collimated monoenergetic beams from Nb cathodes with He gas.

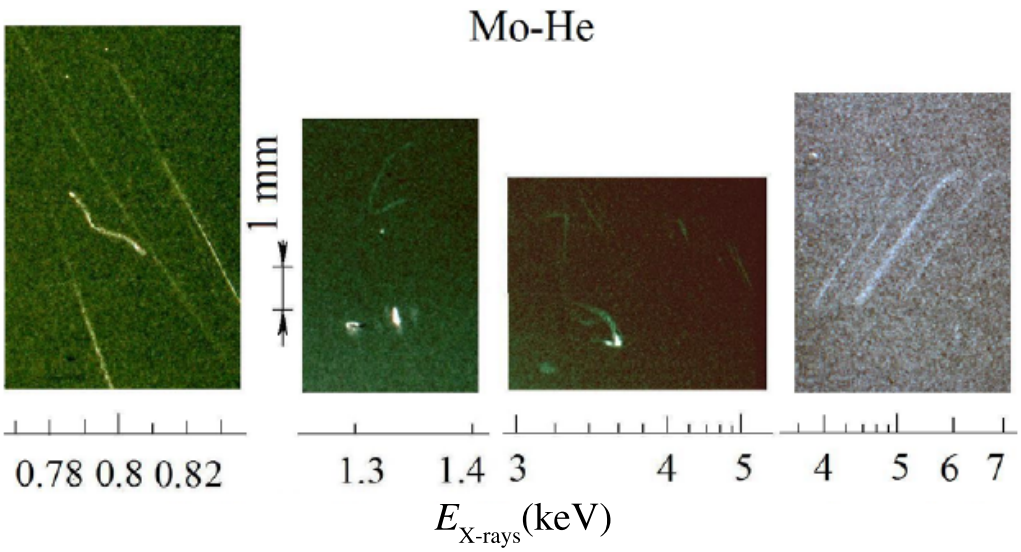

Figure 24. X-ray spectra showing collimated monoenergetic beams from Mo cathodes with He gas.

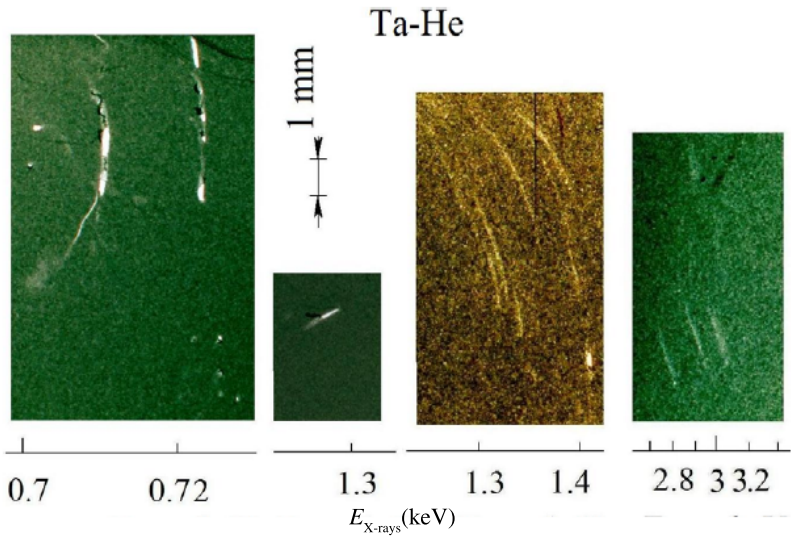

Figure 25. X-ray spectra showing collimated monoenergetic beams from Ta cathodes with He gas.

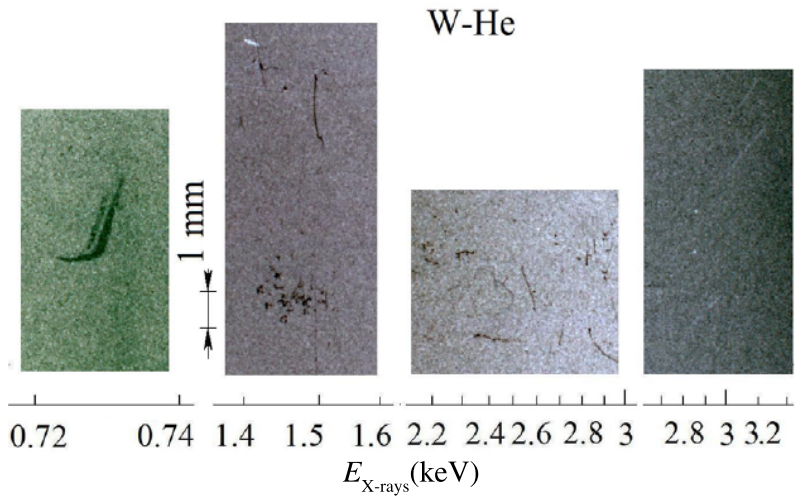

Figure 26. X-ray spectra showing collimated monoenergetic beams from W cathodes with He gas.

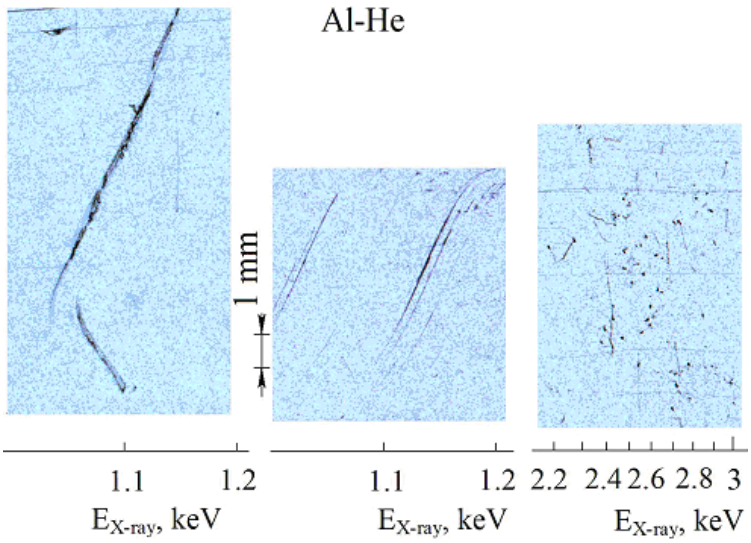

Figure 27. Collimated monoenergetic X-ray beam emission from Al cathodes in He taken after discharge switch off.

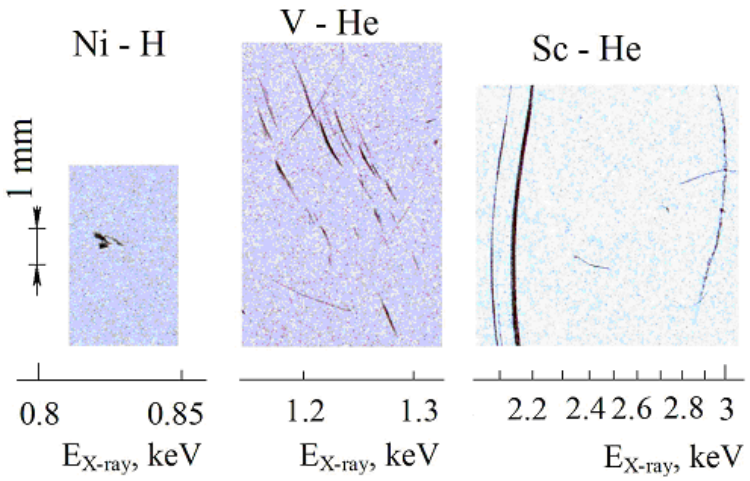

Figure 28. Collimated monoenergetic X-ray beam emission from Ni, V, and Sc cathodes in H_2 and He taken after discharge switch off.

in the modeling, we conclude that this emission is probably not from ^{201}Hg as an impurity in the bulk, but instead is deposited as an impurity from the gas. The coherent energy exchange models show a dynamics that involves a delay for the coherence to build up, and then a rapid energy exchange rate; it may be that the X-ray bursts observed after a delay following discharge switch off is a result of this kind of coherent energy exchange dynamics.

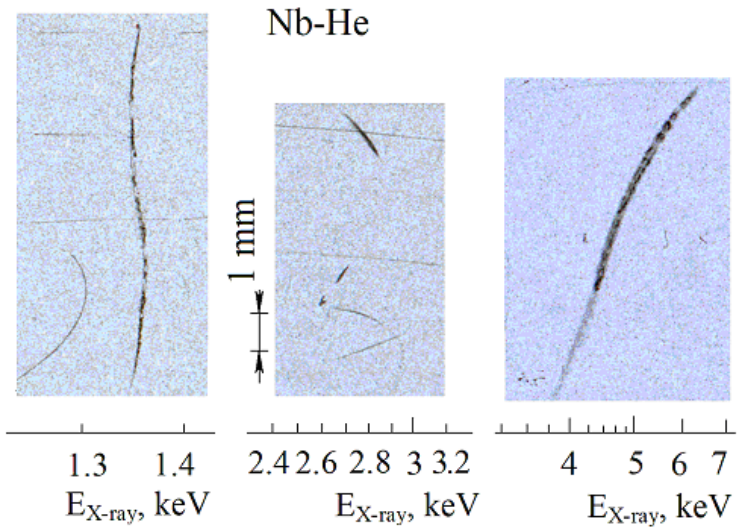

Figure 29. Collimated monoenergetic X-ray beam emission from Nb cathodes in He taken after discharge switch off.

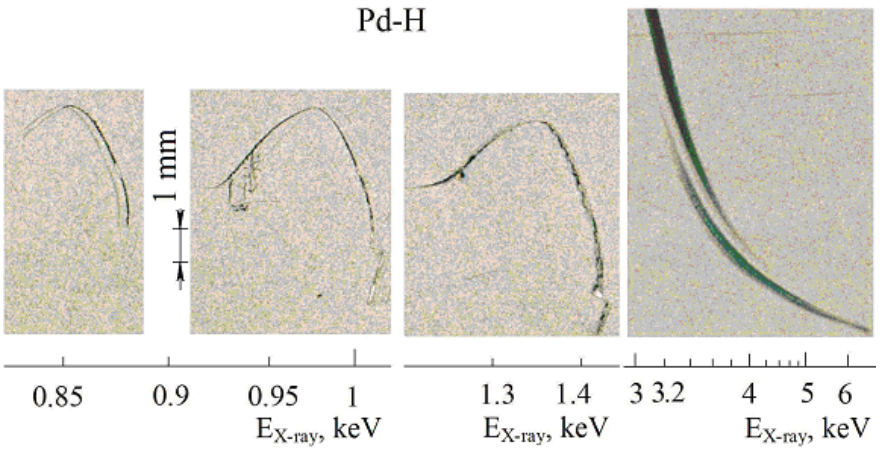

Figure 30. Collimated monoenergetic X-ray beam emission from Pd cathodes in H_2 taken after discharge switch off.

In the case of bursts that occur a long time after the discharge is shut off, it may be that mechanical stimulation of the cathode occurs in connection with the cooling and associated thermal and mechanical relaxation of the cathode assembly.

In the case of diffuse characteristic X-ray emission from gas atoms, the big issue is how excitation occurs. We would expect that the fast electrons should be able to cause inner shell ionization in Ar and Kr, resulting in characteristic X-rays emission. However, this emission in the experiments appears to be localized to the cathode surface or nearby,

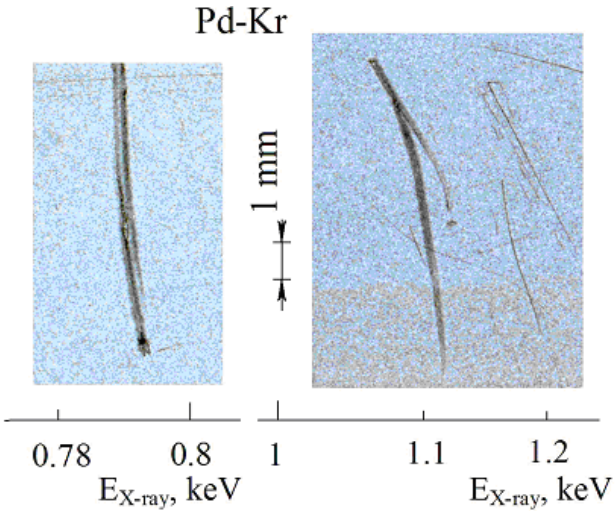

Figure 31. Collimated monoenergetic X-ray beam emission from Pd cathodes in Kr taken after discharge switch off.

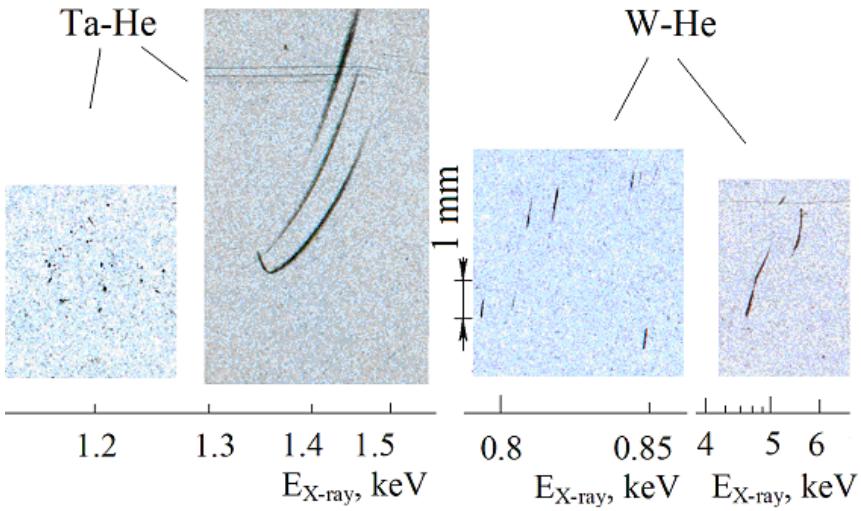

Figure 32. Collimated monoenergetic X-ray beam emission from Ta and W cathodes in He taken after discharge switch off.

while the fast electrons would be expected to produce excitation in an extended region between the cathode and anode. It may be that some Ar and Kr atoms are driven into the outer cathode surface, and are ionized as a result of energy exchange as a result of the spread in the phonon distribution (we have computed the matrix elements for dipole-dipole coupling involving the promotion of an inner shell electron to a phonon-sensitive outer shell orbital, and the coupling matrix elements can be large – in the eV range).

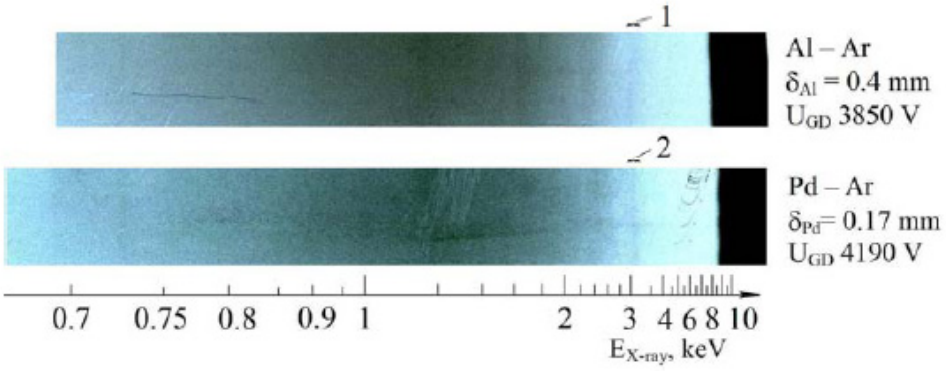

Figure 33. X-ray spectra for Pd and Al cathodes taken in Ar gas showing characteristic K-shell emission (denoted in the spectra as 1 and 2) near 3 keV (the $K_{\alpha 1}$ and $K_{\alpha 2}$ transitions are listed at 2.957 keV and at 2.955 keV). The difference between the observed energy and known energy may be due to the use of the normal incidence grating formula for data analysis.

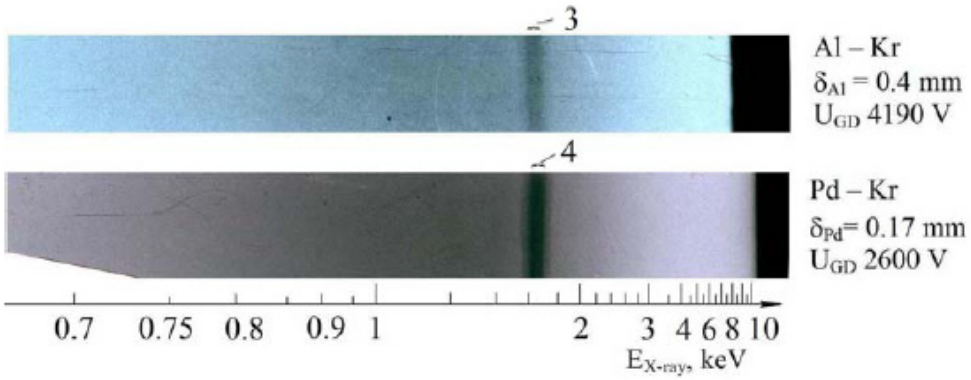

Figure 34. X-ray spectra for Pd and Al cathodes taken in Kr gas showing characteristic L-shell emission (denoted as 3 and 4 in the spectra) near 1.6 keV (the $L_{\alpha 1}$ and $L_{\alpha 2}$ transitions are listed at 1.581 keV and at 1.580 keV). Once again, minor differences between the observed and known energy may be due to the use of the normal incidence grating formula.

Further study is required in order to understand the effect better, and to clarify the connection between the experimental observations and the new models. In light of the X-ray results presented here and the coherent energy exchange models, such future studies might address different specific issues.

For example, collimated emission might be studied using something other than a glow discharge to drive vibrational excitation (such as piezoelectric or pulsed laser stimulation); ^{201}Hg could be ion deposited into the outer surface layer in controlled amounts and controlled depths; and control experiments could be carried out without ^{201}Hg. The emission as a function of vibrational frequency (which could be controlled by the sample thickness) could be investigated. Similar experiments could be carried out based on other low-energy transitions from ground state nuclei (such as the ^{181}Ta transition at 6.24 keV), and the dependence of the number of quanta exchanged could be studies as a function

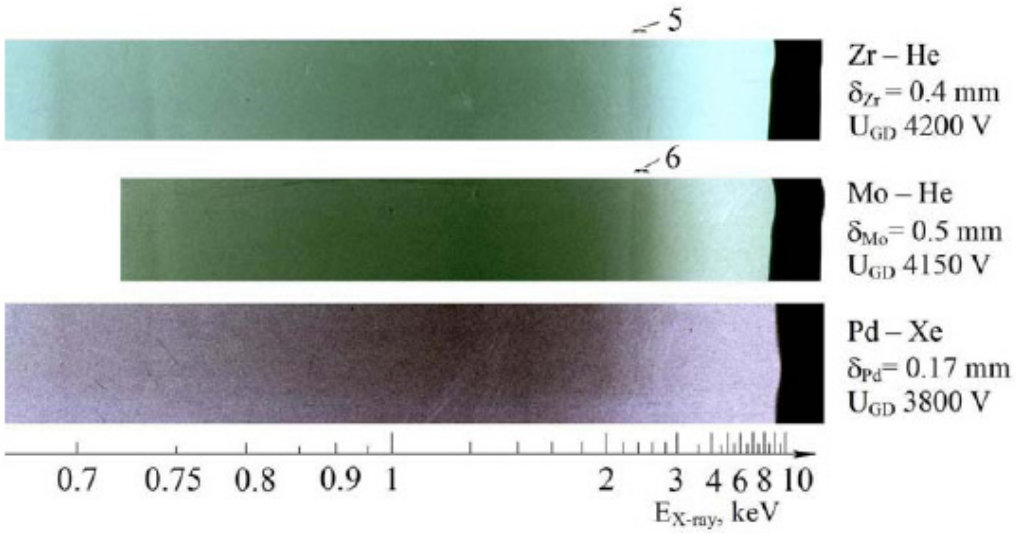

Figure 35. X-ray spectra for Zr, Mo and Pd cathodes taken in He and Xe gas showing characteristic L-shell emission (denoted as 5 and 6 in the spectra) above 2 keV. In the case of Zr, the $L_{\alpha 1}$ and $L_{\alpha 2}$ transitions are listed at 2.042 keV and at 2.040 keV; in the case of Mo, the $L_{\alpha 1}$ and $L_{\alpha 2}$ transitions are listed at 2.293 keV and at 2.290 keV Once again, minor differences between the observed and known energies may be due to the use of the normal incidence grating formula.

of excitation strength. ^{201}Hg could be deposited in plane layers with a known separation in order to maximize the directional output at a particular energy.

Since the diffuse emission seems correlated with the discharge current, it may be that the vibrational modes being excited may be different. In this case, ion bombardment associated with the discharge is effective at driving strong incoherent excitation of very high frequency vibrational modes (in some ways similar to the excitation caused by fluxing hydrogen or deuterium through a metal). Coherent energy exchange with inner shell atomic transitions of impurity atoms could be pursued as a related effect (but one not dependent on, or requiring, ^{201}Hg). It should be possible to correlate the number of quanta exchanged to the level of excitation (presumably the exchange would occur through the most highly excited subset of modes, which would require a statistical analysis to understand); driving the system more strongly should allow higher energy transitions to be excited.

References

[1] A.B. Karabut, Ya. R. Kucherov and I.B. Savvatimova, *Phys. Lett.* A. **170** (1992) 265.
[2] A.B. Karabut, Research into powerful solid X-ray laser (wave length is 0.8–1.2 nm) with excitation of high current glow discharge ions, *Proc. 11th Int. Conf. Emerging Nuclear Energy Systems*, 29 September– 4 October 2002, Albuquerque, New Mexico, USA, pp. 374–381.
[3] A.B. Karabut, Experimental research into characteristics of X-ray emission from solid-state cathode medium of high-current glow discharge, *Proc. 10th Int. Conf. on Cold Fusion*, August 24–29, 2003, Cambridge, MA, USA.
[4] A.B. Karabut, Research into characteristics of X-ray emission laser beams from solid-state cathode medium of high current glow discharge, *Proc. 11th Int. Conf. on Cold Fusion*, 31 October–5 November, 2004, France, pp. 253–257.
[5] A.B. Karabut, Study of energetic and temporal characteristics of X-ray emission from solid state cathode medium of high current glow discharge, *Proc. 12th Int. Conf. on Cold Fusion*, December 2-7, 2006, JAPAN, pp. 344 - 350.

[6] A.B. Karabut and E.A. Karabut, Research into energy spectra of X-ray emission from solid cathode medium during the high current glow discharge operation and after the glow discharge current switch off, *Proc. 14th Int. Conf. on Cold Fusion*, August 10–15, 2008, USA.
[7] A.B. Karabut and E.A. Karabut, Study of deuterium loading into Pd cathode samples of glow discharge, *Proc. of 9th Int. Workshop on Anomalies in Hydrogen/Deuterium Gas Loaded Metals*, 6–11 September 2010, Siena, Italy.
[8] D. Lapraz, P. Iacconi , Y. Sayandi, P. Keller, J. Barthe and G. Portal, *Phys. Stat. Sol.* (A) **108** (1988) 783.
[9] P. Pokorny and A. Ibarra, *J. Appl. Phys.* 7**5** (1994) 1088.
[10] M. Semaan and C. Quarles, *Phys. Rev.* A **24** (1981) 2280.
[11] C. Quarles and M. Semaan, *Phys. Rev.* A **26** (1982) 3147.
[12] D. Roet, C. Ceballos and P. Van Espen, *Nucl. Instr. and Methods Phys. Res.* B **251** (2006) 317.
[13] P.L. Hagelstein and I.U. Chaudhary, *J. Cond. Mat. Nucl. Sci.* **5** (2011) 52.
[14] P.L. Hagelstein and I.U. Chaudhary, *J. Cond. Mat. Nucl. Sci*. **5** (2011) 116.
[15] P.L. Hagelstein, Bird's eye view of phonon models for excess heat in Fleischmann–Pons experiments, this proceedings.
[16] P.L. Hagelstein and I.U. Chaudhary, *J. Cond. Mat. Nucl. Sci.* **5** (2011) 140.
[17] V. Meot, J. Aupiais, P. Morel, G. Gosselin, F. Gobet, J.N. Scheurer, and M. Tarisien, *Phys. Rev.* C **75** (2007) 064306.